Comparison of Optical Coherence Tomography Angiography and Indocyanine Green Angiography in Uveitis

Shilpa Kodati (shilpa.kodati@nih.gov)
National Eye Institute, National Institutes of Health
Aman Kumar
National Eye Institute, National Institutes of Health
Wijak Kongwattananon
National Eye Institute, National Institutes of Health
Susan Vitale
National Eye Institute, National Institutes of Health
Hatice Nida Sen
National Eye Institute, National Institutes of Health

Research Article

Keywords:

Posted Date: March 10th, 2022

DOI: https://doi.org/10.21203/rs.3.rs-1405821/v1

Abstract

Optical Coherence Tomography Angiography (OCTA) has emerged as a useful modality for the diagnosis and management of uveitic diseases, but comparisons with other imaging modalities in uveitis are limited. The purpose of this study is to compare hypocyanescent lesions on Indocyanine Green Angiography (ICGA) to choriocapillaris flow deficits on OCTA in eyes with posterior and panuveitis. En-face 6x6 OCTA images of the choriocapillaris and mid-phase ICGA images from patients with posterior and panuveitis were reviewed and images were quantitatively compared. Lesion(s) on ICGA and OCTA images were outlined, binarized and then overlapped to determine the Dice similarity coefficient (DSC). Measurements of lesion morphology were compared using Bland-Altman analysis contrasting four primary features: lesion number (LN), lesion density (LD%), lesion circularity (LCi) and mean lesion size (MLS). A total of 36 eyes from 26 patients were analyzed. The overall agreement in spatial overlap between lesions from ICG and OCTA was classified as “good” [DSC ≥ 0.7] (mean DSC = 0.744; 95% confidence interval [0.679, 0.809]). No significant differences were noted between the LN, LD%, LCi, and MLS. Overall, OCTA appears to be comparable measure of choriocapillaris flow deficits in patients with posterior and panuveitis compared with hypocyanescent lesions on ICGA.

Introduction

Uveitis is responsible for an estimated 30,000 new cases of legal blindness annually in the United States.[1,2] Dye-based methods including indocyanine green angiography (ICGA) and fluorescein angiography (FA) are part of the standard for evaluating patients with posterior segment uveitis.[3–5]

Optical coherence tomography angiography (OCTA) is an imaging modality that acquires volumetric scans that can be segmented to visualize blood flow at the levels of the retinal capillary plexuses and choriocapillaris at a fixed point in time.[6] Prior reports have described the utility of OCTA in demonstrating changes in the choriocapillaris in patients with posterior segment uveitic diseases including birdshot chorioretinopathy, multifocal choroiditis, punctate inner choroidopathy, and tubercular choroiditis.[7–9] On en-face representations, OCTA can depict areas of choriocapillaris flow deficits and has demonstrated repeatability in uveitis patients.[10] The choriocapillaris flow deficits may represent absent flow or areas of flow that are too slow to be detectable by the OCTA platform.[11–13] Further, OCTA has the advantages of being a non-invasive imaging modality with a relatively short acquisition time that could be well utilized in the clinical setting.

The goal of this study is to investigate the agreement between OCTA and ICGA in assessing choriocapillaris involvement in uveitis patients. We quantitatively evaluated and compared the similarity between choriocapillaris flow deficits on OCTA and hypocyanescent areas on ICGA in patients with posterior and panuveitis.

Methods

Study Design.

A retrospective review of OCTA and ICGA images was conducted of patients diagnosed with posterior and panuveitis and evaluated by the uveitis service at the National Eye Institute (NEI), National Institutes of Health (NIH) Bethesda, MD between December 2016 to August 2021. All research was conducted under an Institutional Review Board (IRB) approved protocol where informed consent for the inclusion for the use of data was obtained by all study participants. This study adhered to the tenets of the Declaration of Helsinki.

Anatomical diagnosis was made based on the Standardization of Uveitis Nomenclature (SUN) criteria.[14] Demographic and clinical data including age, sex, best corrected visual acuity (BCVA) in LogMAR, spherical equivalent (S.E.), disease duration, disease activity were obtained.

Inclusion and exclusion criteria.

Eyes with posterior and panuveitis and with hypocyanescent lesions present on mid-phase ICGA were included. OCTA images obtained on the same date were compared with ICGA. Exclusion criteria were as follows: 1) OCTA image with signal strength < 7; 2) substantial motion artifact or segmentation error; 3) co-existent retinal and choroidal diseases other than uveitis including age-related macular degeneration or central serous chorioretinopathy, and 4) eyes with previous history of macular laser. Structural en-face OCTA images were reviewed to exclude false flow deficits.

Image acquisition.

The ICGA and OCTA images were obtained using the Spectralis HRA, (Heidelberg, Germany) and the CIRRUS AngioPlex Model 5000, (Carl Zeiss Meditec, Germany), respectively. On OCTA, only 6 X 6-mm scans centered on the fovea were included. For quantitative and qualitative interpretation of OCTA images, maximum projection was used to construct the *en*-face representations of the choriocapillaris slab. We defined the choriocapillaris slab at the default setting (29–49 μm below the retinal pigment epithelium (RPE)-fit segmentation line, an estimate of Bruch's membrane).[15] If improper automated segmentation was noted, manual corrections were performed accordingly.

Image processing and analysis.

To quantify the agreement between choriocapillaris flow deficits on OCTA and hypocyanescent lesions on ICGA, a novel semi-automatic algorithm was developed. Each image was graded independently from the corresponding imaging modality. Throughout, the grader was blinded to the patient's diagnosis.

First, images were imported into ImageJ (version 1.51g, National Institutes of Health, Bethesda, MD). Next, the en-face superficial capillary plexus (SCP) OCTA image was opened alongside the ICGA image for feature-based image registration. Image registration is the process of aligning two images to determine corresponding points.[16] Points are often utilized for the basis of registration and were placed on distinctive vessel junctions at corresponding locations.[17,18] A single point was placed in each quadrant of the image for a total of four per image (Fig. 1a,b). Moving Least Squares (MLS) is an automatic, non-rigid, point-based technique in which two images are aligned based on feature points extracted from them.[19] Using the similarity MLS deformation technique (Plugins > Registration > Moving Least Squares > Similarity method), the OCTA image was registered to the ICGA image (Fig. 1c). Image registration was validated by careful visual inspection.

Using the freehand selection tool in ImageJ, hypocyanescent lesions on ICGA images (Fig. 1d,e) or were meticulously outlined (in magenta) and added to the region of interest (ROI) manager. The lesion outlines on each image were filled, and the image was binarized (Fig. 1f). The process was repeated for choriocapillaris flow deficits on OCTA images (Fig. 1g,h,i). To determine the spatial overlap between the lesion areas, the Dice Similarity coefficient (DSC) was computed (Fig. 2). The DSC measures the spatial overlap between two segmentations.[20] A value closer to 0 indicates no spatial overlap between two sets of binary images, and a value of 1, indicates complete overlap.[21] Good agreement was considered if the DSC ≥ 0.7, moderate agreement if the DSC was between 0.5 and 0.7, and poor agreement if the DSC ≤ 0.5, as similarly reported in the literature.[22] The DSC was calculated using the CLIJ2 plugin on ImageJ.[23]

To characterize lesion morphology the “Analyze particles” function on ImageJ was applied to measure the lesion number (LN), mean lesion size (MLS), lesion density (LD%), and the lesion circularity index (LCi). LN is the number of distinct lesions in each image. MLS describes the average lesion size in each image. LD% is the proportion of lesion area to the total image area. LCi quantifies the mean circularity of the lesions in the image, where for any lesion, a value of 1.0 indicates a perfect circle and a value approaching 0.0 indicates an increasingly elongated shape.

Statistical methods.

Statistical analysis was performed using GraphPad Prism version 9.1.2 (GraphPad Software Inc, La Jolla, CA) and. The Anderson-Darling test was performed to detect the normality of distribution. Given their distribution, lesion morphology measurements (LN, MLS, LD% and LCi) obtained from both modalities were compared using the non-parametric Clustered Wilcoxon signed rank test.[24] At the eye level, Bland-Altman plots were used to compare the differences in lesion morphology between OCTA and ICGA against the average of each measurement. Limits of agreement were set to ± 1.96 standard deviations from the mean difference for each morphological feature. To compare the DSC between the clinically active and clinically quiet eyes, Welch’s t-test was selected. The chosen level of statistical significance for all tests was *P* less than 0.05. Mean and SD are reported as “mean ± SD”.

Results

Study population.

A total of 36 eyes from 26 patients (18 female and 8 male) with posterior or panuveitis were included in this study. The mean age was 47.1 ± 13.0 years. Punctate inner choroidopathy (PIC; n = 11 eyes) or serpiginous choroiditis (SC; n = 7 eyes) were the most common disease etiology. The mean disease duration was 7.46 ± 5.58 years (n = 34). The mean BCVA was 0.178 ± 0.298 (Snellen 20/30). The mean S.E. was − 2.13 ± 4.05 (n = 34) and high myopia (S.E. < -6) was seen in four eyes of four patients. Two-thirds of eyes (n = 24) were clinically quiet. Baseline characteristics are listed in Table 1.

Table 1
Baseline characteristics of patients with posterior and panuveitis.

Characteristic	Value
Age, years (mean ± SD)	47.1 ± 13.0
Sex, persons (female: male)	18:8
BCVA, logMAR (mean ± SD)	0.177 ± 0.298
*Disease duration, years (mean ± SD)	7.46 ± 5.58
*Spherical equivalent, diopters (mean ± SD)	-2.13 ± 4.05
Clinical activity, eyes, (quiet: active)	24:12
Disease, eyes 36	
Punctate Inner Choroidopathy	12
Serpiginous Choroiditis	7
Ampiginous Choroiditis	5
Birdshot Chorioretinopathy	5
Vogt-Koyanagi-Harada	2
Idiopathic Panuveitis	2
Multifocal Choroiditis	2
Sarcoid Panuveitis	1

*Best corrected visual acuity (BCVA) and Spherical equivalence included 34 eyes. Values are mean ± standard deviation. LogMAR indicates Logarithm of the Minimum Angle of Resolution.

Measuring spatial agreement between OCTA and ICGA using the DSC.

The mean DSC between all ICGA and OCTA images was 0.744 ± 0.192. Good agreement (0.858 ± 0.092) was seen in 23 (64%) eyes, moderate agreement (0.626 ± 0.069) was seen in nine (25%) eyes, and poor agreement (0.352 ± 0.090) was seen in four (11%) eyes. Among disease subtypes, eyes with SC had the highest mean agreement (0.957 ± 0.024, Fig. 3). Disease etiology was variable in eyes with poor agreement, including: a single eye with sarcoid panuveitis (DSC = 0.244), one of five eyes with ampiginous choroiditis (AC) (DSC = 0.445), and two of twelve eyes with PIC disease (DSC = 0.402 and 0.315).

Comparison of lesion morphology features between OCTA and ICGA.

The distribution of values for lesion features departed from normality and non-parametric testing was chosen for analysis. No significant differences were observed in any of the morphological parameters between the two modalities (P = 0.202 (LN), 0.916 (LD%), 0.178 (MLS), 0.279 (LCi), Clustered Wilcoxon signed-rank test). The mean LN, LD%, MLS, and LCi were 4.00 ± 4.91, 15.5 ± 14.7, 2.49 ± 2.82 mm^2, and 0.585 ± 0.105 in the OCTA group compared with the ICGA group (4.69 ± 4.64, 15.48 ± 14.4, 2.34 ± 3.28 mm^2, and 0.600 ± 0.113). Lesion morphology measurements are summarized in Table 2.

Table 2
Comparison of lesion morphology between imaging modalities.

	OCTA	ICGA	*P-value
LN	4.00 ± 4.91	4.69 ± 4.64	0.202
Active	3.50 ± 3.45	4.67 ± 5.26	0.413
Quiet	4.25 ± 5.55	4.71 ± 4.42	0.318
LD,%	15.5 ± 14.7	15.48 ± 14.4	0.916
Active	8.35 ± 11.6	8.10 ± 9.94	0.716
Quiet	19.0 ± 14.9	19.1 ± 15.0	0.841
MLS, mm^2	2.49 ± 2.82	2.34 ± 3.28	0.178
Active	1.20 ± 1.32	1.73 ± 3.68	0.860
Quiet	3.14 ± 3.15	2.65 ± 3.10	0.097
LCi, (0–1)	0.585 ± 0.105	0.600 ± 0.113	0.279
Active	0.624 ± 0.063	0.611 ± 0.100	0.967
Quiet	0.565 ± 0.117	0.594 ± 0.120	0.191

Lesion morphology was described using four features: lesion number (LN); lesion density (LD), mean lesion size (MLS), and lesion circularity index (LCi). Overall analysis found no significant difference was noted for all morphological features between imaging modalities ($P > 0.05$, n = 36). Subanalysis by disease activity, active (n = 12) or quiet (n = 24) disease, reported similar findings. *Clustered Wilcoxon matched pairs signed-rank test. Values are represented as mean ± standard deviation. OCTA indicates optical coherence tomography angiography. ICGA indicates indocyanine green angiography.

To further assess the comparability between both modalities, Bland-Altman analysis was performed on all morphological features (Fig. 4). Linear regression was performed to analyze for the presence of heteroscedasticity where agreement between the methods decreases as the size of the deviation increases between measurements. There was a mean difference of 0.694 ± 2.80 for LN (Fig. 4a) and − 0.015 ± 0.105 for LCi (Fig. 4b). The 95% limits of agreement (LoA) were between 4.79 and − 6.18 for LN and between 0.192 and − 0.221 for LCi. Regression (slope [95% CI]) demonstrated no significant proportional bias for LN or LCi (0.104 [-0.150 to 0.274]; $R^2 = 0.010$, $P = 0.558$; 0.189 [-0.473 to 0.295]; $R^2 = 0.007$; $P = 0.640$). There was a mean difference of 0.023 ± 3.12 for LD% (Fig. 4c) and 0.149 ± 2.60 mm^2 for MLS (Fig. 4d). The 95% limits of agreement (LoA) for were between 6.15 and − 6.10 for LD% and between 5.24 mm^2 and − 4.94 mm^2 for MLS. Regression demonstrated no significant proportional bias for LD% or MLS (0.021 [-0.054 to 0.096]; $R^2 = 0.009$; $P = 0.572$; -0.183 [-0.504 to 0.137]; $R^2 = 0.038$; $P = 0.253$). Across all morphological features, we noted a total of nine outliers from seven eyes. Two eyes had SC, four eyes had PIC and one eye had AC.

Disease activity and lesion agreement.

Eyes with clinically active disease (0.642 ± 0.175, n = 12) had a significantly lower DSC compared with those eyes with clinically quiet disease (0.789 ± 0.183, n = 24) (*P* = 0.028, Welch's t-test). Figure 5 shows two eyes with PIC with active and quiet disease. Figure 5a,b illustrates a patient eye with active PIC disease where LN was greater on ICGA compared with OCTA and with poor agreement (DSC = 0.402). Figure 5c,d. illustrates a patient eye with no difference in lesion number and good agreement (DSC = 0.817). Lesion morphological features were compared within the active and quiet groups between the two modalities and no significant differences were noted for any of the lesion morphological features within each group. Subanalysis of lesion morphology by disease activity is listed in Table 2.

Discussion

In this retrospective, cross-sectional study, we quantitatively compared choriocapillaris flow deficits on OCTA to hypocyanescent lesions on ICGA in eyes with posterior and panuveitis. We found good agreement in the spatial overlap of hypocyanescent lesions on ICGA with choriocapillaris flow deficits on OCTA. However, agreement between the modalities was significantly lower in the active disease group compared with the quiet group. However, specific aspects of lesion morphology, including the LN, MLS, LD% and LCi, were comparable between OCTA and ICGA.

ICGA has become an established technique to identify and monitor choroidal and retinal diseases.[25,26] However, dye-based angiography is time-consuming, expensive, and invasive with the potential for adverse reactions to these procedures.[27] In contrast, OCTA permits rapid, non-invasive three-dimensional visualization of the choroid and has emerged as an useful imaging modality in the diagnosis and monitoring of patients with uveitis.

OCTA relies on temporal changes in the OCT signal caused by the motion of flow particles, erythrocytes, to discriminate from static tissue. This is followed by device amplitude decorrelation and phase variance methods which enable visualization of the microvasculature, or rather vascular flow.[13,28] Flow deficits on OCTA are thought to be due to ischemia of the choriocapillaris, loss of the choriocapillaris [29] or the result of inflammatory infiltration into the choriocapillaris. [30–33] The inflamed choroid may cause capillary compression resulting in absent or reduced blood flow that is below the detectable threshold on the OCTA device, appearing as a flow deficit.

Few studies have compared flow deficits on OCTA with hypocyanescent lesions seen on ICGA in uveitis. Pepple et al. evaluated three patients with BCR using swept-source OCTA and found that choriocapillaris flow voids colocalized with hypocyanescent ICGA lesions. [34] They also observed regressed flow void after treatment in patients with acute BCR. Similarly, a consistent finding between hypofluorescent lesions in ICGA and flow deficits on OCTA were also demonstrated in active VKH patients.[35] However, comparisons in these studies are largely descriptive. To further validate the utility of OCTA in the uveitis clinic, a quantitative comparison with conventional angiography, ICGA, is necessary.

We used the DSC to quantify the spatial overlap of lesions and demonstrated good agreement between ICGA and OCTA. Further analysis of all disease subtypes included in this study, showed that eyes with SC were found to consistently have the highest level of agreement. This finding correlates with observations in prior studies. Pakzad-Vaezi et al. evaluated the choriocapillaris in patients with a diagnosis of SC using SS-OCTA and compared findings with conventional imaging modalities. In their study, the lesion size and location of choroidal lesion had high agreement between SS-OCTA and ICGA..[36] The high-level agreement in our cohort for SC patients is likely due to the nature of the disease which is chronic and the well demarcated areas of extensive chorioretinal atrophy. These lesions have well-defined borders on OCTA, visualized by their hyperreflective edges and view of underlying medium choroidal vessels, that correlate well with clearly demarcated edges of hypocyanescent lesions on ICGA.[37,38]

Eyes with active disease had significantly lower DSC compared to quiet eyes. However, there was no significant difference in lesion morphology between the modalities for active or quiet disease. In the chronic stage of disease, we observed that the choroidal lesions were atrophic and well-demarcated. In contrast, in the more active phase of disease, the irregularity in the lesions including their borders, and the outer retinal involvement may have contributed to the variability between the two modalities. Notably, in two of the four DSC outliers, hypocyanescent areas due to blockage from outer retinal inflammatory lesions were observed. However, corresponding false flow voids at the level of the choriocapillaris were not seen on OCTA.

Our study is limited by its retrospective nature and relatively small sample size so the study may not have had sufficient power to detect a meaningful difference. Additionally, we only included macular centered images in our study, thus lesions extending to the periphery of the 6 X 6-mm scan, resulted in borders of the captured lesions being defined by the scan area. Wide-field swept-source angiography (SS-OCTA) imaging may capture more peripheral choriocapillaris lesions with higher resolution images, making the comparison between these modalities more representative. Despite limitations, the study included a heterogenous group of uveitic diseases and utilized a unique registration method followed by comprehensive morphological analysis of the lesions.

To our knowledge, this is the first study to extensively compare OCTA and ICGA in the detection of choriocapillaris lesions in posterior and panuveitis. Our results showed that OCTA can be used as a noninvasive imaging modality to visualize choriocapillaris flow deficits which matched hypocyanescent lesions seen on ICGA spatially and morphologically. OCTA can be useful as a tool to detect and monitor choriocapillaris involvement in uveitis, particularly in the macular area, which is significant for visual function. Larger studies with prospective data, and higher resolution OCTA devices with montaging capabilities to permit wider fields of view are necessary for expanding the potential role of OCTA in uveitis management.

Declarations

Author Contributions

An original research manuscript has been submitted to *Scientific Reports* journal. All authors have read the present manuscript and approved to submit. All authors have made a substantial contribution to the manuscript. AK, WK and SK conceived and designed the study. Data collection was performed by AK. Data analysis was performed by AK, WK and SK. SV gave statistical advice during data analysis. AK and WK drafted the manuscript, and was critically revised by SK, HNS and SV.

Data availability:

Raw data was generated at National Eye Institute. The data that support the findings of this study are available from the corresponding author, SK, upon reasonable request.

Additional Information

Competing Interests:

The author(s) declare no competing interests.

References

1. Acharya, N. R. *et al.* Incidence and prevalence of uveitis: results from the Pacific Ocular Inflammation Study. *JAMA Ophthalmol.* **131**, 1405–1412 (2013).
2. Nussenblatt, R. B. The natural history of uveitis. *Int. Ophthalmol.* **14**, 303–308 (1990).
3. Flower, R. W., Fryczkowski, A. W. & McLeod, D. S. Variability in choriocapillaris blood flow distribution. *Invest. Ophthalmol. Vis. Sci.* **36**, 1247–1258 (1995).
4. Herbort, C. P. Posterior uveitis: new. *Eye* **12**, 757–759 (1998).
5. Howe, L., Stanford, M., Graham, E. & Marshall, J. Indocyanine green angiography in inflammatory eye disease. *Eye* **12 (Pt 5)**, 761–767 (1998).
6. de Carlo, T. E., Romano, A., Waheed, N. K. & Duker, J. S. A review of optical coherence tomography angiography (OCTA). *Int J Retina Vitreous* **1**, 5 (2015).
7. Khan, H. A. & Jahangir, S. Evolving evidence about the role of choriocapillaris in pathogenesis of uveitis. *Acta Scientific Ophthalmology* **4**, (2021).
8. Hassan, M. *et al.* The Role of Optical Coherence Tomography Angiography in the Management of Uveitis. *Int. Ophthalmol. Clin.* **56**, 1–24 (Fall 2016).
9. Pichi, F. *et al.* The application of optical coherence tomography angiography in uveitis and inflammatory eye diseases. *Prog. Retin. Eye Res.* **59**, 178–201 (2017).
10. Caplash, S. *et al.* Repeatability of optical coherence tomography angiography in uveitic eyes. *Transl. Vis. Sci. Technol.* **8**, 17 (2019).

11. Greig, E. C., Duker, J. S. & Waheed, N. K. A practical guide to optical coherence tomography angiography interpretation. *Int J Retina Vitreous* **6**, 55 (2020).
12. Zhang, Q. *et al.* Accurate estimation of choriocapillaris flow deficits beyond normal intercapillary spacing with swept source OCT angiography. *Quantitative Imaging in Medicine and Surgery* **8**, 658–666 (2018).
13. Spaide, R. F., Fujimoto, J. G., Waheed, N. K., Sadda, S. R. & Staurenghi, G. Optical coherence tomography angiography. *Prog. Retin. Eye Res.* **64**, 1–55 (2018).
14. Jabs, D. A., Nussenblatt, R. B., Rosenbaum, J. T. & Standardization of Uveitis Nomenclature (SUN) Working Group. Standardization of uveitis nomenclature for reporting clinical data. Results of the First International Workshop. *Am. J. Ophthalmol.* **140**, 509–516 (2005).
15. Rosenfeld, P. J. *et al.* ZEISS Angioplex^{TM} Spectral Domain Optical Coherence Tomography Angiography: Technical Aspects. *Dev. Ophthalmol.* **56**, 18–29 (2016).
16. Sathyanarayanan, V. & Bodenheimer, R. E. Evaluation of moving least squares as a technique for non-rigid medical image registration. in *Medical Imaging 2009: Image Processing* vol. 7259 823–833 (SPIE, 2009).
17. Akbarzadeh, A. *et al.* Evaluation of whole-body MR to CT deformable image registration. *J. Appl. Clin. Med. Phys.* **14**, 4163 (2013).
18. Zitová, B. & Flusser, J. Image registration methods: a survey. *Image Vis. Comput.* **21**, 977–1000 (2003).
19. Schaefer, S., McPhail, T. & Warren, J. Image deformation using moving least squares. *ACM Trans. Graph.* **25**, 533–540 (2006).
20. Dice, L. R. Measures of the amount of ecologic association between species. *Ecology* **26**, 297–302 (1945).
21. Zou, K. H. *et al.* Statistical validation of image segmentation quality based on a spatial overlap index. *Acad. Radiol.* **11**, 178–189 (2004).
22. Zijdenbos, A. P., Dawant, B. M., Margolin, R. A. & Palmer, A. C. Morphometric analysis of white matter lesions in MR images: method and validation. *IEEE Trans. Med. Imaging* **13**, 716–724 (1994).
23. Haase, R. *et al.* CLIJ: GPU-accelerated image processing for everyone. *Nat. Methods* **17**, 5–6 (2020).
24. Rosner, B., Glynn, R. J. & Lee, M.-L. T. The Wilcoxon signed rank test for paired comparisons of clustered data. *Biometrics* **62**, 185–192 (2006).
25. Flower, R. W. & Hochheimer, B. F. A clinical technique and apparatus for simultaneous angiography of the separate retinal and choroidal circulations. *Invest. Ophthalmol.* **12**, 248–261 (1973).
26. Cimino, L., Auer, C. & Herbort, C. P. Sensitivity of indocyanine green angiography for the follow-up of active inflammatory choriocapillaropathies. *Ocul. Immunol. Inflamm.* **8**, 275–283 (2000).
27. Meira, J., Marques, M. L., Falcão-Reis, F., Rebelo Gomes, E. & Carneiro, Â. Immediate Reactions to Fluorescein and Indocyanine Green in Retinal Angiography: Review of Literature and Proposal for Patient's Evaluation. *Clin. Ophthalmol.* **14**, 171–178 (2020).

28. Cerquaglia, A. *et al.* New Insights On Ocular Sarcoidosis: An Optical Coherence Tomography Angiography Study. *Ocul. Immunol. Inflamm.* **27**, 1057–1066 (2019).
29. Waheed, N. K., Moult, E. M., Fujimoto, J. G. & Rosenfeld, P. J. Optical Coherence Tomography Angiography of Dry Age-Related Macular Degeneration. *Dev. Ophthalmol.* **56**, 91–100 (2016).
30. Dick, A. D. & Carter, D. A. Cytokines and immunopathogenesis of intraocular posterior segment inflammation. *Ocul. Immunol. Inflamm.* **11**, 17–28 (2003).
31. Mrejen, S., Sarraf, D., Chexal, S., Wald, K. & Freund, K. B. Choroidal Involvement in Acute Posterior Multifocal Placoid Pigment Epitheliopathy. *Ophthalmic Surg. Lasers Imaging Retina* **47**, 20–26 (2016).
32. Rao, N. A. Pathology of Vogt-Koyanagi-Harada disease. *Int. Ophthalmol.* **27**, 81–85 (2007).
33. Karampelas, M. *et al.* Choroidal assessment in idiopathic panuveitis using optical coherence tomography. *Graefes Arch. Clin. Exp. Ophthalmol.* **251**, 2029–2036 (2013).
34. Pepple, K. L. *et al.* Use of En Face Swept-Source Optical Coherence Tomography Angiography in Identifying Choroidal Flow Voids in 3 Patients With Birdshot Chorioretinopathy. *JAMA Ophthalmol.* **136**, 1288–1292 (2018).
35. Aggarwal, K. *et al.* The Role of Optical Coherence Tomography Angiography in the Diagnosis and Management of Acute Vogt-Koyanagi-Harada Disease. *Ocul. Immunol. Inflamm.* **26**, 142–153 (2018).
36. Pakzad-Vaezi, K. *et al.* Swept-Source OCT Angiography of Serpiginous Choroiditis. *Ophthalmol Retina* **2**, 712–719 (2018).
37. McKay, K. M. *et al.* Automated Quantification of Choriocapillaris Lesion Area in Patients with Posterior Uveitis. *Am. J. Ophthalmol.* (2021).
38. Mandadi, S. K. R. *et al.* Novel findings on optical coherence tomography angiography in patients with tubercular serpiginous-like choroiditis. *Retina* **37**, 1647–1659 (2017).

Figures

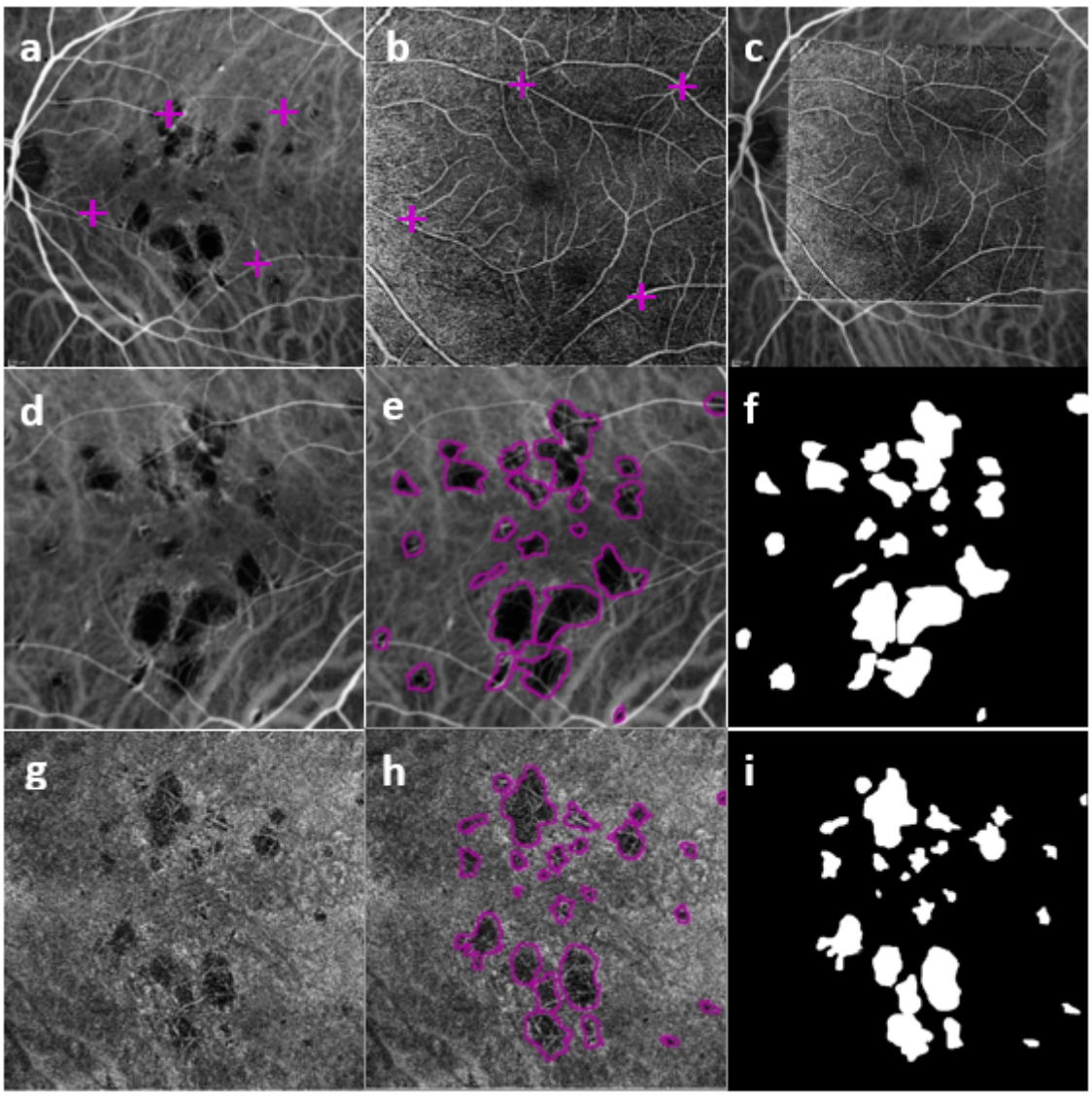

Figure 1

Example image registration between OCTA and ICGA images. OCTA images were registered to mid-phase ICGA images to allow for lesion comparison for each eye. A point (magenta) was placed on a vessel junction in each quadrant of the (**a**) ICGA and the (**b**) en-face SCP OCTA images at corresponding locations. Registration was completed using a feature-based similarity MLS registration method on ImageJ that resulted in the image (**c**). The individual lesions on the (**d**) ICGA image were (**e**) outlined by the grader and the image was (**f**) binarized . The same procedure was repeated for the (**g,h,i**) OCTA image. The binarized images were used for further analysis of lesion overlap and morphology comparison between the two imaging modalities. OCTA indicates optical coherence tomography angiography. ICGA indicates indocyanine green angiography. SCP indicates superficial capillary plexus. MLS indicates mean least squares.

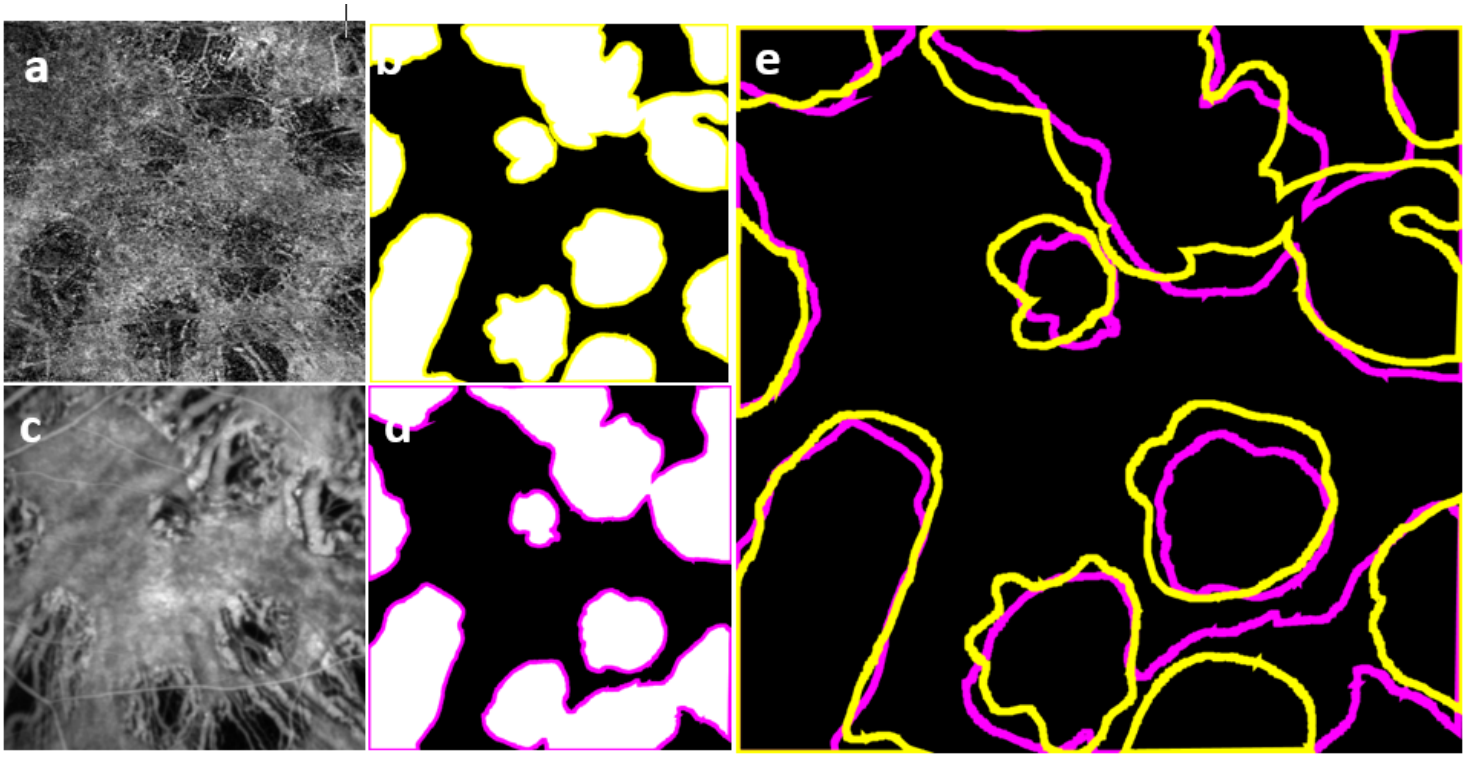

Figure 2

Example of Dice-similarity coefficient (DSC) computation. After binarization of the grader-annotated lesions on the en-face choriocapillaris OCTA image (**a,b**) and the ICGA image (**c,d**), lesions were overlapped using ImageJ (**e**). Lesion outlines on the en-face choriocapillaris OCTA image are represented in yellow. Lesion outlines on the ICGA image are represented in magenta. DSC is calculated as two times the area of overlap divided by the total number of pixels in both images. OCTA indicates optical coherence tomography angiography. ICGA indicates indocyanine green angiography. DSC indicates Dice-similarity coefficient.

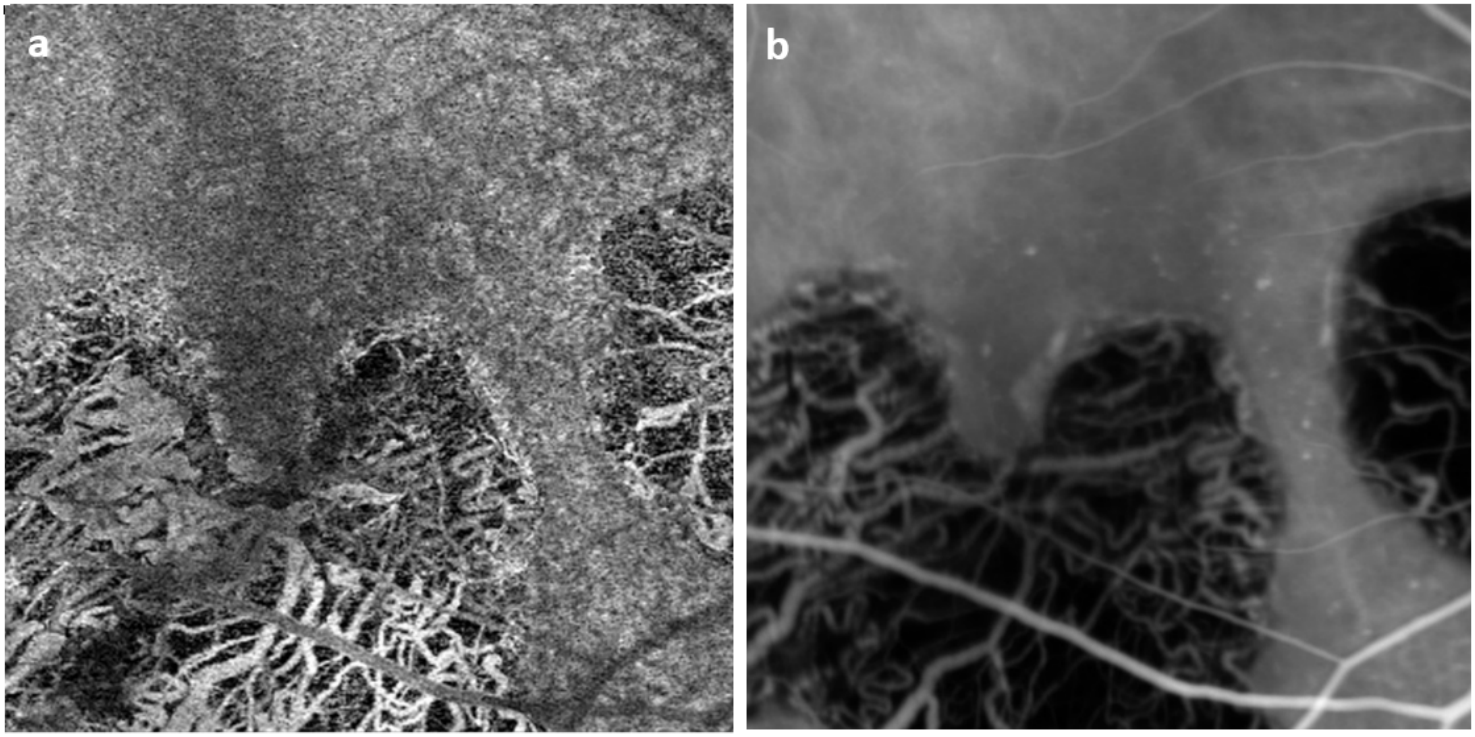

Figure 3

Eyes with Serpiginous Choroiditis (SC) had the highest mean Dice-similarity coefficient (DSC) among all disease subtypes. Example of an eye with SC. Image registered(**a**) en-face choriocapillaris OCTA image and (**b**) ICGA image. Choroidal atrophy is seen with well demarcated lesion borders. The mean DSC for patients with SC was 0.957 ± 0.024 (n=7). Good agreement was defined as DSC ≥ 0.7. OCTA indicates optical coherence tomography angiography. ICGA indicates indocyanine green angiography.

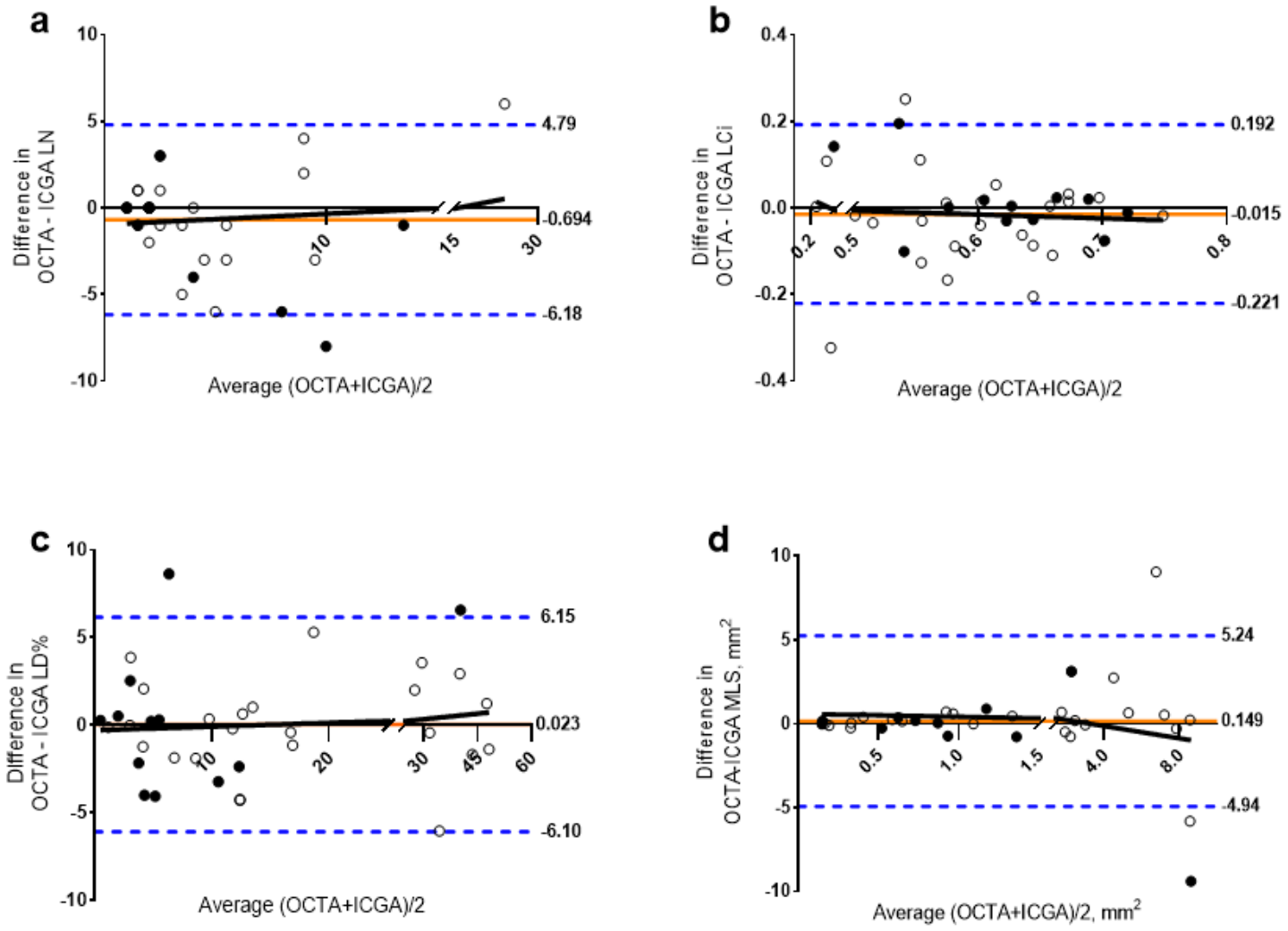

Figure 4

Bland-Altman comparison between the morphological characteristics of lesions between OCTA and ICGA images. (**a**) Lesion number (LN) (**b**) Lesion circularity (LCi) (**c**) Lesion density (LD%) (**d**) Mean lesion size (MLS). The orange solid horizontal line represents the mean difference for each parameter across all images. The blue dotted horizontal lines represent the upper (mean + 2 SD) and lower limits (mean − 2 SD) that define the interval of agreement where 95% of the differences between the two modalities lie. The black solid line represents the linear regression line and analysis of differences and mean for all parameters used to evaluate for proportional bias between the modalities. The filled points indicate eyes with active disease and the hollow points indicate eyes with quiet disease. The differences between LN, LD%, and LCi were normally distributed between the two modalities. However, the differences between MLS were not normally distributed. OCTA indicates optical coherence tomography angiography. ICGA indicates indocyanine green angiography. SD indicates standard deviation.

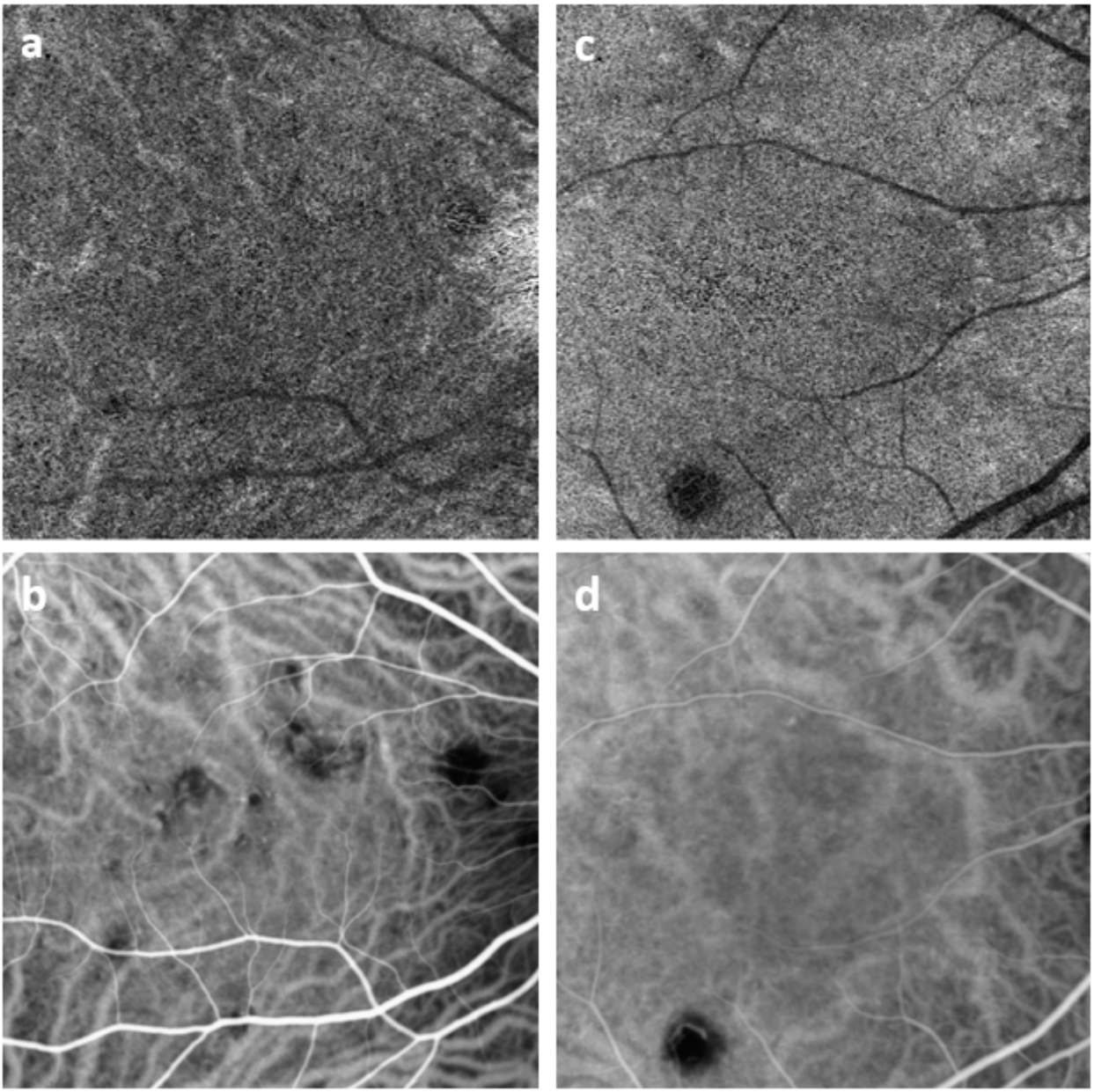

Figure 5

Disease activity and DSC analysis. An example of an eye with poor agreement (DSC ≤ 0.5) between modalities and an eye with good agreement (DSC ≥ 0.7). En-face choriocapillaris OCTA images (top row) with their corresponding ICGA images below (bottom row). Eye with active PIC disease demonstrating fewer LN on OCTA (**a**) compared with ICGA (**b**) and poor agreement (DSC = 0.402). (**c,d**) Eye with quiet PIC disease demonstrating no difference in LN and good agreement (DSC = 0.817). PIC indicates punctate inner choroidopathy. OCTA indicates optical coherence tomography angiography. ICGA indicates indocyanine green angiography. DSC indicates Dice-similarity coefficient. LN indicates lesion number.